

RSC Advances



This is an *Accepted Manuscript*, which has been through the Royal Society of Chemistry peer review process and has been accepted for publication.

Accepted Manuscripts are published online shortly after acceptance, before technical editing, formatting and proof reading. Using this free service, authors can make their results available to the community, in citable form, before we publish the edited article. This *Accepted Manuscript* will be replaced by the edited, formatted and paginated article as soon as this is available.

You can find more information about *Accepted Manuscripts* in the [Information for Authors](#).

Please note that technical editing may introduce minor changes to the text and/or graphics, which may alter content. The journal's standard [Terms & Conditions](#) and the [Ethical guidelines](#) still apply. In no event shall the Royal Society of Chemistry be held responsible for any errors or omissions in this *Accepted Manuscript* or any consequences arising from the use of any information it contains.



Journal Name

ARTICLE

Controllable Synthesis of CdS/WO₃ Heterostructures with Enhanced Photoelectrochemical Performance

Received 00th January 20xx,
Accepted 00th January 20xx

Yi Liu,^{a*} Yingde Cui,^b Feiyan Huang,^a and Xinzhe Yang^a

DOI: 10.1039/x0xx00000x

www.rsc.org/

With the increasing energy and environmental problems, photoelectrochemical (PEC) water splitting has recently attracted a great deal of attention. Herein, we report the facile synthesis of CdS/WO₃ heterostructures as high-performance photoanodes for PEC water splitting. CdS/WO₃ heterostructures are successfully prepared on F doped SnO₂ glass substrates by a two-step process, which involves a hydrothermal growth and electrochemical deposition process. In comparison to pristine WO₃ nanostructures, CdS/WO₃ heterostructures exhibit substantially high harvesting ability. The CdS/WO₃ heterostructures yield a significant photocurrent density of 1.8 mA cm⁻² at 0 V vs. Ag/AgCl, which is substantially higher than that of bare WO₃ and CdS electrodes. These findings will open up new opportunities to develop other efficient solar-light-driven photocatalytic cells.

Introduction

As the energy crisis and environmental pollution getting more and more serious, hydrogen, has attracted enormous amount of research attention as a clean energy because its product of combustion is just water and bring no greenhouse gases.¹⁻³ Among various methods to produce hydrogen, one of the most promising and environmental friendly ways is photoelectrochemical (PEC) water splitting over the semiconductors.⁴⁻⁹ Tungsten trioxide (WO₃), with a band gap of around 2.6 eV, is of great interest due to its excellent intrinsic stability, environmental compatibility and excellent solar-to-chemical performance under the visible light irradiation.¹⁰⁻¹⁵ However, some key drawbacks of WO₃ photoanodes, such as relatively high recombination of the photo-generated electron-hole pairs and low absorption coefficient of visible light, have severely limited their practical applications.^{10, 16, 17} Several strategies have been explored to reduce electron-hole recombination in WO₃, including nanostructuring and doping with transition elements.^{11, 12, 16, 18, 19} However, the efficiency is still not satisfactory and it is urgency to find proper approaches to enhance the PEC performance of the WO₃ photoanodes.

Sulfides are emerging as attractive visible-light-driven photocatalysts since they have narrow band gaps with suitable conduction bands at relatively high potentials.²⁰⁻²⁴ Among them, CdS is one of the most attractive II-VI group semiconductors with a direct band gap of 2.4 eV, which has

been extensively studied in photocatalytic hydrogen production and the photo-degradation due to its strong ability for harvesting visible light.^{23, 25-29} Considerable efforts have been devoted to enhance the photo-catalytic activity of WO₃ by combining it with the CdS, and some achievements have been successfully made.³⁰⁻³³ However, there are few reports about the PEC performance of the CdS/WO₃ heterostructures. Thus, it is highly desirable to investigate the properties of CdS/WO₃ heterostructures for their PEC water splitting. Herein, we demonstrated the design and synthesis of CdS/WO₃ heterostructures on F doped SnO₂ (FTO) glass substrates, following by studying their PEC water splitting. The CdS/WO₃ heterostructures exhibited a significant photocurrent density of 1.8 mA cm⁻² at 0 V vs. Ag/AgCl with good stability. These findings will open up new opportunities to develop other efficient solar-light-driven photocatalytic cells.

Results and discussion,

X-ray powder diffraction (XRD) analysis was conducted to identify the crystalline phase of the products. Figure 1a shows the typical XRD spectra of the WO₃ and CdS/WO₃ samples. All of the reflections of the XRD pattern for WO₃ sample could be indexed to monoclinic WO₃ with a lattice constant a = 7.297 Å, b = 7.539 Å and c = 7.688 Å, compatible with JCPDS Card No. 43-1035. The diffraction peaks rose at diffraction angle of 23.1°, 23.6°, 24.4°, 33.3°, 34.2°, 55.6° and 56.0° corresponding to (002), (020), (200), (022), (202), (140) and (420) planes were observed, indicating good crystallinity of the as-prepared WO₃ sample. The strong diffraction peaks of SnO₂ at 26.7°, 33.9°, 37.9° and 51.7° come from FTO substrate. No other obvious peaks were obtained, demonstrating that high purity of the WO₃. The SEM image of a typical WO₃ nanostructure is presented in Figure 1b. Many nanosheets constituted with some small nanoparticles were observed. The width of the nanosheets was around 500 nm. After the electro-deposition at the potential of -1.0 V vs. Ag/AgCl for 300 s at room

^a School of Chemistry and Chemical Engineering, Guangdong Pharmaceutical University, Guangzhou 510006, China E-mail: liuyi915@126.com

^b Guangzhou Vocational College of Science and Technology, Guangzhou, Guangdong 510550, China

† Footnotes relating to the title and/or authors should appear here.

Electronic Supplementary Information (ESI) available: [details of any supplementary information available should be included here]. See DOI: 10.1039/x0xx00000x

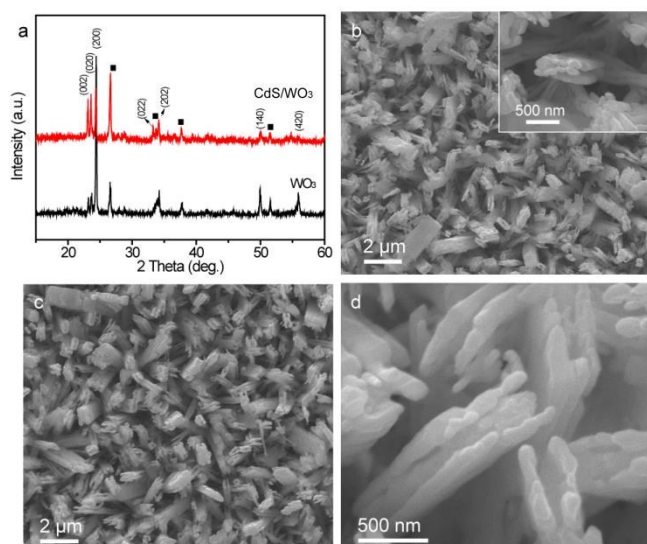


Figure 1. (a) XRD patterns of pure WO_3 and CdS/WO_3 heterostructures. SEM images of: (b) pure WO_3 , (c-d) CdS/WO_3 heterostructures.

temperature, the CdS/WO_3 heterostructures were prepared. No characteristic peaks corresponding to CdS were observed, which may be due to the amorphous structures and/or the low intensity of the CdS. It is noteworthy that the width of the CdS/WO_3 heterostructures is also closed to 500 nm, suggesting that a thin CdS layer was constructed on the surface of WO_3 (Figure 1c-d).

In order to better understand the microstructure of CdS/WO_3 heterostructures, transmission electron microscopy (TEM) was conducted and displayed in Figure 2. It shows that the WO_3 was covered by a shell of CdS. SAED analysis clearly demonstrate that both the CdS and WO_3 have high degree of crystallinity (Figure 2b). Figure 2c is the high-resolution TEM (HR-TEM) image taken from the rectangle part of the CdS/WO_3 (Figure 2a). The lattice spacing of 0.37 nm and 0.38 nm match well with the (020) and (002) lattice spacing of monoclinic structure WO_3 (JCPDS Card No. 43-1035). In addition, the well-resolved lattice space of 0.24 nm corresponds to the interplanar spacing of (102) plane of hexagonal CdS (JCPDS Card No. 65-3414). Therefore, CdS/WO_3 heterostructures are successfully synthesized.

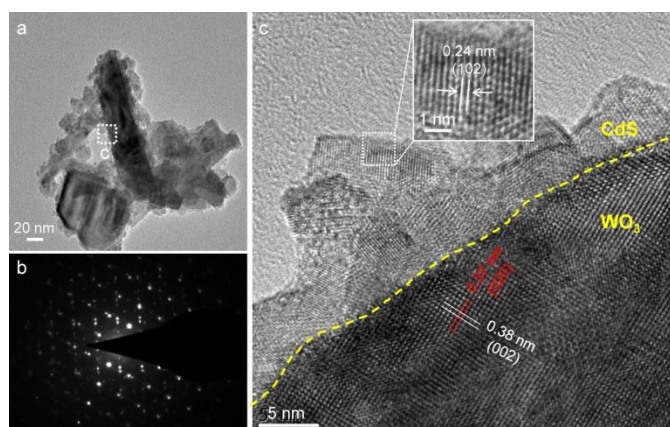


Figure 2. TEM image, (b) SAED pattern and (c) HR-TEM image of the CdS/WO_3 heterostructures.

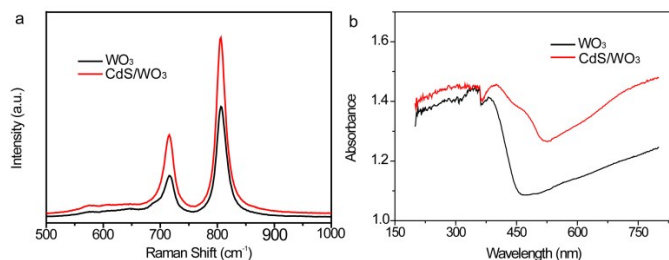


Figure 3. (a) Raman and (b) UV-Vis spectra of pure WO_3 and CdS/WO_3 heterostructures.

As presented in Figure 3a, Raman spectra of WO_3 sample showed well defined bands at 715 and 808 cm^{-1} corresponding to the monoclinic phase of tungsten oxide. Both these two characteristic peaks originate from the O-W-O bending modes and stretching modes.³⁴ No obvious peaks can be assigned to CdS. The UV-Vis absorption spectra of bare WO_3 and CdS/WO_3 heterostructures were measured in order to reveal the influence of the CdS. As shown in Figure 3b, the WO_3 have a shape absorption edge around 450 nm, which is consistent with its band gap of 2.6 eV.¹⁶ On the other hand, it has a visible light absorption from 450 to 560 nm due to the strong absorption of CdS in the visible region. The absorption edge of the CdS/WO_3 heterostructures shifts to 580 nm due to the strong absorption of the CdS in the visible region. Hence, the surface of WO_3 nanostructures was successfully coated with a visible-light absorption material of CdS.

X-ray photoelectron spectroscopy (XPS) analysis was also conducted to study the composition of pure WO_3 and CdS/WO_3 heterostructures, which is presented in Figure 4. Figure 4a compares the XPS survey spectra of the pure WO_3 and CdS/WO_3 heterostructures. In comparison to pure WO_3 , the XPS survey spectrum of CdS/WO_3 heterostructure shows additional peaks of S and Cd, which demonstrates the formation of CdS. Additionally, the atom ratio of Cd, S, W and O in these CdS/WO_3 heterostructures is about 4.51%, 3.74%, 13.13% and 37.94%, respectively. The ratio of W to O is closed to the chemical formula of WO_3 , while the ratio of Cd to S is higher than 1, suggesting that Cd is slightly rich than S in our sample. Figure 4b displays the W 3d core level XPS spectra. After coating with CdS, the intensity of the W was decreased, indicating the CdS is generated at the surface of the WO_3 nanostructures. The Cd 3d core level XPS spectrum of CdS/WO_3 sample is showed in Figure 4c. Two obvious peaks located at 404.9 and 411.7 eV are observed, which are consistent with the reported values for Cd^{2+} .³⁵ As shown in Figure 4d, the S 2p core level XPS spectrum can be deconvoluted to two peaks. The peaks centered at 161.3 and 162.4 eV are attributed to the S 2p_{3/2} and S 2p_{2/1} of S²⁻.³⁶ All these results clearly confirm that the successful preparation of the CdS/WO_3 heterostructures, which consists with the XRD and TEM analyses.

Because the nanostructure can provide high pathway for the electron transport, well-aligned nanostructure with narrow band gap is very promising and efficient for the conversion of solar energy.⁸ Therefore, the as-prepared CdS/WO_3 heterostructures are used as photoanodes in a PEC cell. For better comparison, pristine CdS electrode was prepared by directly using FTO as substrate at the same synthetic condition with CdS/WO_3 electrode. The PEC activities of bare WO_3 ,

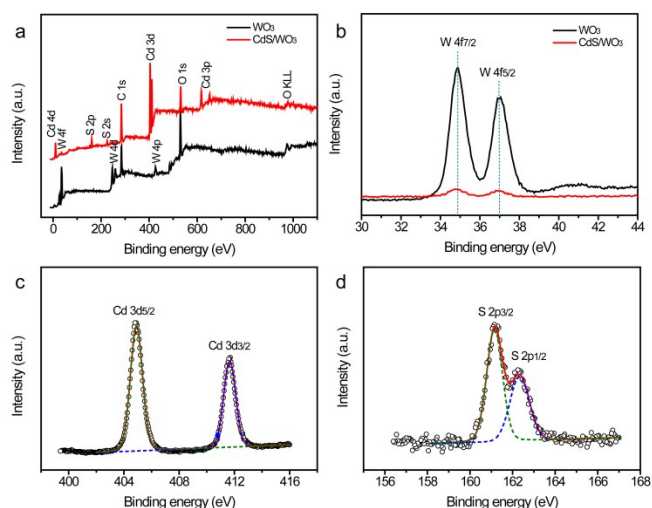


Figure 4. (a) XPS survey spectrum, (b) W 4f, (c) Cd 3d, and (d) O 1s core level XPS spectrum of the pure WO_3 and CdS/WO_3 heterostructures.

CdS and CdS/WO_3 photoelectrodes were firstly characterized by measuring the linear sweep voltammogram (LSV) curves with or without light irradiation. As presented in Figure 5a, the scans for all the samples collected in the potential range from -1.0 V to 0.2 V vs. Ag/AgCl showed a negligible background current without light irradiation. In contrast, under the light illumination, all the samples showed pronounced photocurrent. It is noteworthy that the CdS/WO_3 electrode achieved a remarkable photocurrent density of 1.8 mA cm^{-2} at the potential of 0 V vs. Ag/AgCl , which is substantially higher than that of bare WO_3 (0.8 mA cm^{-2}) and CdS (0.6 mA cm^{-2}) electrodes at the same potential. Such the enhancement of photocurrent for the CdS/WO_3 heterostructures can be attributed to the improvement of light-harvesting (Figure 3b).

The incident photon-to-current conversion efficiency (IPCE) of the samples was measured in the solution of 0.1 M Na_2S and 0.1 M Na_2SO_3 at -0.2 V vs. Ag/AgCl in order to quantitatively investigate the relation between the light absorption and the PEC performance. As shown in Figure 5b, the maximum IPCE value of the bare WO_3 electrode is approximately 23% at the wavelength of 340 nm and then it gradually decrease ranging from 350 to 450 nm and to almost zero at $\lambda > 500 \text{ nm}$ last, indicating that the band gap of WO_3 is ca. 2.6 eV. As for the bare CdS electrode, its maximum IPCE is about 19% and it showed a higher IPCE value than that of the WO_3 electrode at the wavelength of 380-550 nm, revealing the superior photoactivity of CdS under visible light. Significantly, the IPCE value of the CdS/WO_3 heterostructures was up to ca. 67%, much higher than the WO_3 and CdS samples. It also shows remarkable photo response of 23 % at 450 nm and gradually decreases to zero at 550 nm. All these results above fully confirm that the synergistic effect of CdS layer and WO_3 nanostructures can significantly enhance the photoelectrochemical activity of the CdS/WO_3 heterostructures.

Beside photocurrent, stability is another one of important parameters to evaluate the performance of the photoanode. The current-time (i-t) chronoamperometric response of the WO_3 , CdS and CdS/WO_3 photoanodes at a potential of 0 V vs. Ag/AgCl were collected in Figure 5c. Obviously, the

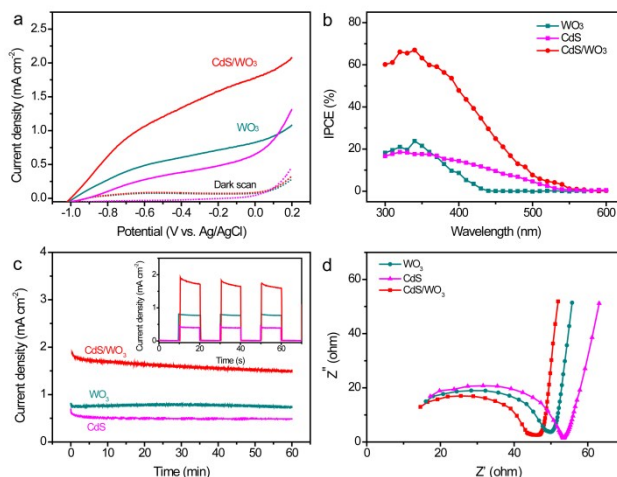


Figure 5. (a) LSV curves collected at 50 mV s^{-1} under dark and light irradiation and (b) IPCE curves at the incident wavelength ranging from 300 to 600 nm for the WO_3 , CdS and CdS/WO_3 samples in a solution of 0.1 M Na_2S and 0.1 M Na_2SO_3 . (c) Photocurrent density of the CdS , WO_3 and CdS/WO_3 photoanodes as a function of irradiation time collected at 0 V vs. Ag/AgCl . Inset is its corresponding temporal photocurrent responses at 0 V vs. Ag/AgCl . (d) Nyquist plots of the WO_3 , CdS and CdS/WO_3 electrodes under light irradiation.

CdS/WO_3 electrode exhibited remarkably higher photocurrent than that of the bare WO_3 and CdS electrodes during the long-term test, again showing the outstanding photoelectrochemical performance of CdS/WO_3 heterostructures. The bare CdS electrode remained only 69.8% of its initial photocurrent after 60 min under light irradiation. In contrast, the CdS/WO_3 electrode showed enhanced stability that can retain more than 80.1% of its initial photocurrent density. This indicates that the construction of heterostructures can improve the stability of CdS . On the other hand, we also collected the temporal photocurrent response of all photoanodes at the potential of 0 V vs. Ag/AgCl . It can be seen from the inset in Figure 5c that the current of the CdS/WO_3 electrode suffered from a relatively sharp decrease at the initial short time and then remained stable. This temporal decrease might be due to the recombination of photo-generated charge carriers by the surface (or defect) states of the CdS/WO_3 heterostructures.³⁷

Electrochemical impedance spectroscopy (EIS) spectra of the WO_3 , CdS and CdS/WO_3 electrodes under light irradiation were collected to further understand the charge-transfer and separation properties of the hetero-structures, as shown in Figure 5d. The radius of the arc is correlated with the charge-transfer ability at the corresponding electrode/electrolyte interface. A smaller radius correlated with a lower charge-transfer resistance and an effective separation of photo-generated electron-hole pairs.³⁹ The arc radius of CdS/WO_3 heterostructures is obviously reduced compared to those of both the CdS and WO_3 under light irradiation, which means an effective interfacial charge transfer and charge separation.

Conclusions

In summary, we have designed and synthesized the CdS/WO_3 heterostructures for the PEC water splitting. The images of SEM and TEM indicated that the CdS/WO_3 heterostructures were successfully prepared, and the UV-Vis absorption spectra showed an obvious

red-shift of the absorption edge. Under the light illumination, the CdS/WO₃ heterostructures achieved a significant photocurrent density of 1.8 mA cm⁻² at the potential 0 V vs. Ag/AgCl, which is much larger than that of the bare WO₃ and CdS electrodes at the same potential. The IPCE spectra also show the enhanced photo-response in the visible region. These results suggest that the heterostructures can greatly enhance the photoactivity of the WO₃ nanostructures. This achievement makes it possible to design composite photoelectrodes to more effectively utilize the solar spectrum.

Experimental

Preparation of WO₃ nanostructures: All the reagents used in this study were of analytical grade and were used directly without any purification. The FTO glass was cleaned ultrasonically in ethanol, distilled water, and acetone and finally rinsed in ethanol. The preparation of the WO₃ nanostructures can be found in our previous work.³⁸ In general, 1.8 g H₂WO₄ was dissolved into 35 mL H₂O and 5 mL H₂O₂ (30%) under strong stirring for 4 h. Then, the clear solution was heated at 95 °C with stirring, and further diluted into 40 mL with deionized water. Then, around 4 mL of the precursor was mixed with 16 mL of ethanol and NH₄Cl, and transferred to Teflon-lined stainless steel autoclave. A piece of FTO-glass substrate was sealed into the solution and the autoclave maintained at 180 °C for 10 h. After reaction, the autoclave cooled down naturally to room temperature, and the FTO were washed with deionized water and ethanol for 3 times to remove ions that possibly remained at the final products, following by dried at 60 °C for 12 h.

Synthesis of the CdS quantum dots (CdS QDs): Cadmium acetate and thioacetamide were dissolved separately at a concentration of 10 mM in deionized water at room temperature as precursor solutions. CdS QDs was obtained by mixing precursors with the same volume and aging 30 min before electrochemical deposition.

Synthesis of the CdS/WO₃ heterostructures: The CdS/WO₃ heterostructures were prepared by a facile electrochemical deposition. In a typical synthesis route, chronopotentiometry was carried out in a conventional three-electrode cell with a Pt wire as the counter electrode and a saturated calomel electrode (SCE) serving as the reference electrode. The working electrode was the WO₃ nanostructures on the FTO substrate. The deposition was carried out by applying the potential of -1.0 V vs. Ag/AgCl for 300 s at room temperature. Pristine CdS/FTO electrode was also prepared by using FTO as substrate at the same synthetic condition.

Materials characterizations: The surface morphology, microstructure and the composition of the samples were analyzed by scanning electron microscope (SEM, Quanta 400), transmission electron microscopy (TEM, JEM2010-HR), X-ray diffraction (XRD, D8 ADVANCE) with Cu K α radiation (λ = 1.5418 Å), and X-ray Photoelectron Spectroscopy (XPS, ESCALab250) and the Raman spectroscopy (Raman, RenishawinVia). The optical properties of the samples were measured with a UV-Vis-NIR Spectrophotometer (UV, Shimadzu UV-3150).

Photoelectrochemical characterizations: PEC measurements were carried out in a home-made three-electrode cell with a quartz window to facilitate illumination in a mixed solution of 0.1 M Na₂S and 0.1 Na₂SO₃. The working electrode is the as-

prepared samples, while a Pt wire and a saturated Ag/AgCl electrode was used as the counter electrode and reference electrode, respectively. All photoelectrochemical experiments were measured by a CHI 760D electrochemical station. The illumination source was a 150 W xenon lamp (Newport 69907) with intensity of about 100 mW cm⁻². The incident-photon-to-current-conversion efficiencies (IPCE) were measured with a CHI 760D electrochemical station with a solar simulator (Newport 69911, 300 W xenon lamp) coupled with an aligned monochromator (Oriel Cornerstone 260 1/4 m).

Acknowledgements

This work was supported by the Science and technology project of Guangdong Province (2015A090905013), Guangzhou Yuexiu District Science and Technology Projects Funds (2014-WS-029), Science and technology project of self financing in Guangdong Province.

Notes and references

†Footnotes relating to the main text should appear here. These might include comments relevant to but not central to the matter under discussion, limited experimental and spectral data, and crystallographic data.

§
§§
etc.

1. X. Lu, S. Xie, H. Yang, Y. Tong and H. Ji, *Chem. Soc. Rev.*, 2014, **43**, 7581-7593.
2. M. Li, X. He, Y. Zeng, M. Chen, Z. Zhang, H. Yang, P. Fang, X. Lu and Y. Tong, *Chem. Sci.*, 2015, **6**, 6799-6805.
3. C. Yao, B. Wei, H. Ma, L. Meng, X. Zhang and Q. Gong, *J. Power Sources*, 2013, **237**, 295-299.
4. G. Wang, Y. Ling, H. Wang, L. Xihong and Y. Li, *J. Photochem. Photobiology C: Photochem. Rev.*, 2014, **19**, 35-51.
5. S. Xie, T. Zhai, W. Li, M. Yu, C. Liang, J. Gan, X. Lu and Y. Tong, *Green Chem.*, 2013, **15**, 2434-2440.
6. J.-J. Park, D.-Y. Kim, J.-G. Lee, Y.-H. Cha, M. T. Swihart and S. S. Yoon, *RSC Adv.*, 2014, **4**, 8661-8670.
7. G. Wang, H. Wang, Y. Ling, Y. Tang, X. Yang, R. C. Fitzmorris, C. Wang, J. Z. Zhang and Y. Li, *Nano Lett.*, 2011, **11**, 3026-3033.
8. S. Xie, M. Li, W. Wei, T. Zhai, P. Fang, R. Qiu, X. Lu and Y. Tong, *Nano Energy*, 2014, **10**, 313-321.
9. H. Li, J. Yang, J. Zhang and M. Zhou, *RSC Adv.*, 2012, **2**, 6258-6261.
10. S. S. Kalanur, Y. J. Hwang, S. Y. Chae and O. S. Joo, *J. Mater. Chem. A*, 2013, **1**, 3479-3488.
11. C. Santato, M. Odziemkowski, M. Ulmann and J. Augustynski, *J. Am. Chem. Soc.*, 2001, **123**, 10639-10649.
12. A. Tanaka, K. Hashimoto and H. Kominami, *J. Am. Chem. Soc.*, 2013, **136**, 586-589.
13. G. Hodes, D. Cahen and J. Manassen, *Nature*, 1976, **260**, 312-313.
14. J. Su, L. Guo, N. Bao and C. A. Grimes, *Nano Lett.*, 2011, **11**, 1928-1933.

15. J. Lin, P. Hu, Y. Zhang, M. Fan, Z. He, C. K. Ngaw, J. S. C. Loo, D. Liao and T. T. Y. Tan, *RSC Adv.*, 2013, **3**, 9330-9336.
16. G. Wang, Y. Ling, H. Wang, X. Yang, C. Wang, J. Z. Zhang and Y. Li, *Energy Environ. Sci.*, 2012, **5**, 6180-6187.
17. W. Li, J. Li, X. Wang, J. Ma and Q. Chen, *Int. J. Hydrogen Energy*, 2010, **35**, 13137-13145.
18. F. Zhan, R. Xie, W. Li, J. Li, Y. Yang, Y. Li and Q. Chen, *RSC Adv.*, 2015, **5**, 69753-69760.
19. B. Cole, B. Marsen, E. Miller, Y. Yan, B. To, K. Jones and M. Al-Jassim, *J. Phys. Chem. C*, 2008, **112**, 5213-5220.
20. W. Li, S. Xie, M. Li, X. Ouyang, G. Cui, X. Lu and Y. Tong, *J. Mater. Chem. A*, 2013, **1**, 4190-4193.
21. G. Wang, X. Yang, F. Qian, J. Z. Zhang and Y. Li, *Nano Lett.*, 2010, **10**, 1088-1092.
22. S. Yang, X. Wen, W. Zhang and S. Yang, *J. Electrochem. Soc.*, 2005, **152**, G220-G226.
23. S. Xie, X. Lu, T. Zhai, J. Gan, W. Li, M. Xu, M. Yu, Y.-M. Zhang and Y. Tong, *Langmuir*, 2012, **28**, 10558-10564.
24. H. Li, C. Chen, X. Huang, Y. Leng, M. Hou, X. Xiao, J. Bao, J. You, W. Zhang, Y. Wang, J. Song, Y. Wang, Q. Liu and G. A. Hope, *J. Power Sources*, 2014, **247**, 915-919.
25. W. Li, M. Li, S. Xie, T. Zhai, M. Yu, C. Liang, X. Ouyang, X. Lu, H. Li and Y. Tong, *CrystEngComm*, 2013, **15**, 4212-4216.
26. W. Kim, M. Seol, H. Kim, J. B. Miller, A. J. Gellman and K. Yong, *J. Mater. Chem. A*, 2013, **1**, 9587-9589.
27. W.-T. Sun, Y. Yu, H.-Y. Pan, X.-F. Gao, Q. Chen and L.-M. Peng, *J. Am. Chem. Soc.*, 2008, **130**, 1124-1125.
28. H. Tada, T. Mitsui, T. Kiyonaga, T. Akita and K. Tanaka, *Nat. Mater.*, 2006, **5**, 782-786.
29. H. Li, C. Yao, L. Meng, H. Sun, J. Huang and Q. Gong, *Electrochimica Acta*, 2013, **108**, 45-50.
30. Z.-G. Zhao, Z.-F. Liu and M. Miyauchi, *Adv. Funct. Mater.*, 2010, **20**, 4162-4167.
31. H.-i. Kim, J. Kim, W. Kim and W. Choi, *J. Phys. Chem. C*, 2011, **115**, 9797-9805.
32. H. Kim, Y. Tak, K. Senthil, J. Joo, S. Jeon and K. Yong, *J. Vacuum Sci. & Technol. B*, 2009, **27**, 2182-2186.
33. H. Li, Y. Zhou, L. Chen, W. Luo, Q. Xu, X. Wang, M. Xiao and Z. Zou, *Nanoscale*, 2013, **5**, 11933-11939.
34. M. Boulouva, N. Rosman, P. Bouvier and G. Lucazeau, *J. Phys.: Condensed Matter*, 2002, **14**, 5849.
35. C. Wang, L. Sun, H. Yun, J. Li, Y. Lai and C. Lin, *Nanotechnology*, 2009, **20**, 295601.
36. C. Z. Yao, B. H. Wei, H. X. Ma, H. Li, L. X. Meng, X. S. Zhang and Q. J. Gong, *J. Power Sources*, 2013, **237**, 295-299.
37. Y. Mao, J. He, X. Sun, W. Li, X. Lu, J. Gan, Z. Liu, L. Gong, J. Chen, P. Liu and Y. Tong, *Electrochim. Acta*, 2012, **62**, 1-7.
38. Y. Liu, S. Xie, C. Liu, J. Li, X. Lu and Y. Tong, *J. Power Sources*, 2014, **269**, 98-103.
39. H. Li, Y. Zhou, L. Chen, W. Luo, Q. Xu, X. Wang, M. Xiao, Z. Zou, *Nanoscale*, 2013, **5**, 11933-11939.

Graphical Abstract

